On the Performance of Visible Light Communication Systems With Non-Orthogonal Multiple Access

Hanaa Marshoud, *Student Member, IEEE*, Paschalis C. Sofotasios, *Senior Member, IEEE*, Sami Muhaidat, *Senior Member, IEEE*, George K. Karagiannidis, *Fellow, IEEE*, and Bayan S. Sharif, *Senior Member, IEEE*

***Abstract*— Visible light communication (VLC) has been proposed as a promising and efficient solution to indoor ubiquitous broadband connectivity. In this paper, non-orthogonal multiple access, which has been recently introduced as an effective scheme for fifth generation (5G) wireless networks, is considered in the context of VLC systems under different channel uncertainty models. To this end, we first derive a novel closed-form expression for the bit-error-rate (BER) under perfect channel state information (CSI). Capitalizing on this, we then quantify the effect of noisy and outdated CSI by deriving a simple and accurate approximation for the former and a tight upper bound for the latter. The offered results are corroborated by respective results from extensive Monte Carlo simulations and assist in developing useful insights on the effect of imperfect CSI knowledge on the overall system performance. Furthermore, it was shown that while noisy CSI leads to slight degradation in the BER performance, outdated CSI can cause considerable performance degradation, if the order of the users' channel gains change due to the involved mobility.**

***Index Terms*— Visible light communications, non-orthogonal multiple access, imperfect channel state information, bit-error-rate, dimming control.**

I. Introduction

DRIVEN by the vast growth in the global demand for increased wireless data connectivity and the recent advances in solid-state lighting, visible light communication (VLC) has evolved significantly as a potential candidate to the wireless data explosion dilemma. Based on this, it has recently attracted the attention of both academia and industry as an effective complementing technology to traditional radio frequency (RF) communications [1]–[4]. In VLC systems, light emitting diodes (LEDs) are utilized for data transmission, where the intensity of the LED light is modulated at particularly high switching rate that cannot be perceived by the human eye. This process is known as intensity modulation (IM). Then, at the receiver site, a photo detector (PD) is used to convert the variations in the received light intensity into electrical current that is subsequently used for data recovery [5]–[7].

A. Related Literature

As a promising broadband technology, VLC is expected to provide remarkably high speed indoor communication as well as support ubiquitous connectivity. To this end, several multiple access schemes have been proposed for VLC systems, including carrier sense multiple access (CSMA), orthogonal frequency division multiple access (OFDMA) and code division multiple access (CDMA) [8]. In more details, in CSMA-based systems, each LED is required to sense the channel before attempting to transmit in order to avoid collisions. Yet, when an LED's transmitted signal is undetectable by others, the "hidden terminal" problem arises leading to considerable performance degradation [9]. A full-duplex carrier sense multiple access (FD-CSMA) protocol was proposed in [10] to avoid the "hidden terminal" problem. This is realized by considering downlink transmissions as busy medium for the uplink channel, which in turn reduces the incurred collisions. However, carrier sensing needed for CSMA is not trivial in VLC due to line-of-sight (LOS) transmissions along with the need for request-to-send/clear-to-send (RTS/CTS) symbols, which leads to an overall increased signaling overhead [11].

In the same context, OFDMA is an effective multiple access scheme but it cannot be applied directly to VLC systems due to the restriction for positive and real signals imposed by IM and the illumination requirements. Based on this, DC-biasing and clipping techniques have been proposed in order to adapt OFDMA to VLC systems. To this end, optical orthogonal frequency division multiple access (O-OFDMA) was proposed as a modified OFDMA scheme by asymmetrically clipping the transmitted OFDM signal at zero level in order to satisfy the positivity constraint [12]. The performance of O-OFDMA was then compared to optical orthogonal frequency division multiplexing interleave division multiple access (O-OFDM-IDMA) showing that while O-OFDM-IDMA outperforms O-OFDMA in terms of power efficiency, O-OFDMA exhibits the benefit

Manuscript received July 9, 2016; revised December 6, 2016 and May 5, 2017; accepted June 15, 2017. Date of publication July 11, 2017; date of current version October 9, 2017. This paper was presented in part at the IEEE International Conference on Communications, Paris, France, 2017. The associate editor coordinating the review of this paper and approving it for publication was J. Cheng. *(Corresponding author: Sami Muhaidat.)*

H. Marshoud and B. S. Sharif are with the Department of Electrical and Computer Engineering, Khalifa University, Abu Dhabi 127788, UAE (e-mail: hanaa.marshoud@kustar.ac.ae; bayan.sharif@kustar.ac.ae).

P. C. Sofotasios is with the Department of Electrical and Computer Engineering, Khalifa University, Abu Dhabi 127788, UAE, and also with the Department of Electronics and Communications Engineering, Tampere University of Technology, 33101 Tampere, Finland (e-mail: p.sofotasios@ieee.org).

S. Muhaidat is with the Department of Electrical and Computer Engineering, Khalifa University, Abu Dhabi 127788, UAE, and also with the Institute for Communication Systems, University of Surrey, Guildford GU2 7XH, U.K. (e-mail: muhaidat@ieee.org).

G. K. Karagiannidis is with the Department of Electrical and Computer Engineering, Aristotle University of Thessaloniki, 54 124 Thessaloniki, Greece (e-mail: geokarag@auth.gr).

Color versions of one or more of the figures in this paper are available online at http://ieeexplore.ieee.org.

Digital Object Identifier 10.1109/TWC.2017.2722441

of reduced decoding complexity. Moreover, O-OFDMA provides lower peak-to-average power ratio (PAPR) compared to O-OFDM-IDMA. Yet, adapting OFDMA in order to cope with VLC requirements leads to significant reduction of spectral efficiency, which is a crucial disadvantage in emerging communications that typically require significantly increased throughputs.

In the same context, CDMA is another multiple access scheme that has been proposed for VLC systems, exploiting optical orthogonal codes (OOC) [13], [14] to allow multiple users to access the channel using full spectrum and time resources. Thus, it can provide enhanced spectral efficiency compared to OFDMA. In this context, an experimental optical code-division multiple access (OCDMA) based VLC system was presented in [15] where it was shown that the major drawback of OCDMA is the need for long OOC codes, which leads to a reduction of the theoretically achievable data rates. This issue was addressed in [16] where a code-cycle modulation (CCM) technique was proposed to enhance the spectral efficiency of OCDMA by using different cyclic shifts of the spreading sequence assigned to the different users. Yet, another limitation of OCDMA is the poor correlation characteristics in the OOC codes. This problem was addressed in [17] by means of a synchronization mechanism that aims to improve the performance of OCDMA.

Non-orthogonal multiple access (NOMA) was proposed in [18] as a spectrum-efficient multiple access scheme for downlink VLC systems. In NOMA, the signals of different users are superimposed in the power domain by allocating different power levels based on the channel conditions of each user. Thus, users can share the entire frequency and time resources leading to increased spectral efficiency. NOMA allocates higher power levels to users with worse channel conditions than those with good channel conditions. As a result, the user with the highest allocated power is able to decode directly its signal, while treating the signals of other users as noise. Meanwhile, the other users in the system perform successive interference cancellation (SIC) for the multi-signal separation, prior to decoding their signals. Based on these characteristics, the concept of NOMA has recently gained interest in RF systems as a candidate for 5G and long term evolution advanced (LTE-A) systems [19], [20]. To this effect, the performance of NOMA downlink system with randomly deployed users was investigated in [21], where NOMA was shown to provide improved outage probability when power allocation is carefully designed. However, it was also shown that the performance gains of NOMA are degraded in low signal-to-noise-ratio (SNR) scenarios. In [22], NOMA has been applied to multiple-antenna relaying networks, where the outage behavior of the mobile users was analyzed. It was shown that NOMA leads to improved spectral efficiency and fairness compared to orthogonal multiple access schemes.

Likewise, the application of NOMA in multiple-input-multiple-output (MIMO) configurations has been studied in [23] and [24]. In this context, it is recalled that two types of interference cancellation techniques are required in MIMO-NOMA systems: 1) SIC for the intra-beam demultiplexing of users having the same precoding weights; and 2) inter-beam interference cancellation for users with different precoding weights. Also, the impact of channel state information (CSI) on the performance of NOMA was first examined in [25], where the ergodic capacity maximization problem was considered under total transmit power constraints. Likewise, the outage probability for a downlink NOMA system was thoroughly analyzed in [26], where closed-form expressions were derived for the case of different channel uncertainty models based on imperfect CSI and second order statistics. The performance of NOMA-VLC was analyzed in [27] and [28] in terms of coverage probability and ergodic sum rate and it was shown extensively that NOMA enhances the system capacity compared to time division multiple access (TDMA). Likewise, it was shown in [29] that NOMA also outperforms OFDMA in terms of the achievable data rate in the downlink of VLC systems.

It is noted here that the majority of the reported contributions on optical NOMA assume perfect knowledge of the channel fading coefficients. However, in practical communication scenarios, these coefficients must be first estimated and then used in the detection process. Yet, channel estimation can not always be perfect in practice, which results to subsequent decoding errors that degrade the overall system performance. Motivated by this, VLC channel estimation errors were considered in [30] for the joint optimization of precoder and equalizer in optical MIMO systems, while the impact of noisy CSI on the performance of different MIMO precoding schemes was investigated in [31]. Likewise, the contribution in [32] analyzed the impact of CSI errors on a multiuser VLC downlink network, where the corresponding system performance was evaluated under two channel uncertainty models, namely noisy and outdated CSI.

It is also recalled that in order to consider NOMA in commercial implementations, it is essential to ensure that it satisfies the requirements imposed by the illumination functionality of VLC systems [33]. According to to the IEEE Standard 802.15.7 [34], VLC wireless networks are required to support light dimming in order to allow the control of the perceived light brightness according to the users' preference. Hence, integrating efficient dimming techniques into VLC systems is vital for energy savings as well as for aesthetic and comfort purposes, rendering a wide implementation of VLC systems more rational. Based on this, various dimming methods have been proposed in the literature to incorporate data transmission into dimmable light intensities by means of different modulation and coding schemes. In general, brightness control can be achieved by two different techniques: continuous current reduction (CCR) and pulse-width modulation (PWM). In CCR, also known as analog dimming, dimming control is realized by changing the forward current of the LED, while in PWM, also known as digital dimming, the forward current remains constant while the duty cycle of the signal is varied in order to meet the dimming requirements. Analog and digital dimming have been applied to different modulation schemes in VLC, such as on-off keying (OOK) and pulse position modulation (PPM) [35]. Moreover, dimming control was implemented in a VLC-OFDM system in [36] where it was shown that CCR achieves higher luminous

efficacy, whereas PWM leads to throughput degradation. It is noted here that supporting dimming control in NOMA-VLC systems can be rather challenging because NOMA is fundamentally based on dividing the LED power among the different users in the network, which renders the corresponding system performance highly susceptible to any reduction in transmit power. Based on the above, it is shown in detail that the present work quantifies the impact of channel estimation errors on the performance of indoor NOMA-VLC systems under noisy and outdated channel uncertainty models as well as under analog and digital dimming techniques.

A detailed outline of the contribution of this work is provided in the following subsection.

B. Contribution

In the present paper, we consider NOMA as a multiple access scheme for the downlink of indoor VLC networks. Specifically, the contribution of this paper is summarized below:

1) We investigate the error rate performance of NOMA-VLC systems, and derive an exact analytic expression for the bit-error-rate (BER) for an arbitrary number of users for the case of perfect CSI.
2) We quantify the impact of CSI errors on the system performance under two channel uncertainty models, namely noisy CSI, and outdated CSI that may result from the mobility of the indoor users. In this context, we derive a closed-form approximate expression for the BER under noisy CSI, as well as a tight upper bound for the BER under outdated CSI.
3) We analyze the effect of dimming support on the BER performance of NOMA-VLC systems. In particular, two different dimming schemes are considered: OOK analog dimming and variable OOK (VOOK) dimming.

To the best of our knowledge, the above topics have not been previously investigated in the open technical literature, including related analyses in conventional radio communications.

C. Structure

The remainder of the paper is organized as follows: Section II describes the channel and system model of an indoor VLC downlink network. Section III analyzes the BER performance under perfect CSI, while Section IV investigates the performance of NOMA under two different cases for CSI errors. Section V discusses the performance of NOMA-VLC under dimming control while numerical results and related discussion are presented in Section VI. Finally, closing remarks are provided in Section VII.

II. Channel and System Model

We consider a single-LED downlink VLC system deployed in an indoor environment. The LED has a dual function of illumination and communication, and serves N users simultaneously by modulating the intensity of the emitted light according to the data received through a power line communications (PLC) backbone network. Also, all users are equipped with a single PD, that performs direct detection to extract the transmitted signal from the received optical carrier. This is realized by considering unipolar OOK modulation due to its popularity in VLC systems [34], [37] and the references therein.

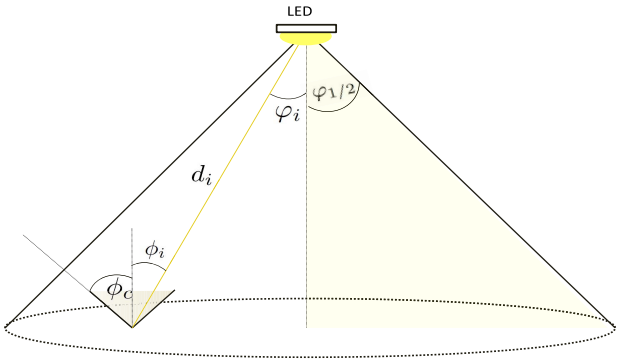

Fig. 1. VLC channel model.

A. The VLC Channel

The current set up is based on LOS communication scenarios as illustrated in Fig. 1, since multipath delays resulting from reflections and diffuse refractions are typically negligible in indoor VLC settings [38]. The channel between user U_i and the corresponding LED is given by

$$h_i = \begin{cases} \frac{A_i}{d_i^2} R_o(\varphi_i) T_s(\phi_i) g(\phi_i) \cos(\phi_i), & 0 \le \phi_i \le \phi_c \\ 0, & \phi_i > \phi_c \end{cases} \quad (1)$$

where i =1, 2, 3, …, N, A_i represents the receiver PD area, d_i accounts for the distance between the transmitting LED and the i-th receiving PD, φ_i is the angle of emergence with respect to the transmitter axis, ϕ_i is the angle of incidence with respect to the receiver axis, ϕ_c is the field of view (FOV) of the PD, $T_s(\phi_i)$ is the gain of the optical filter and $g(\phi_i)$ is the gain of the optical concentrator, which is expressed as

$$g(\phi_i) = \begin{cases} \frac{n^2}{\sin^2(\phi_c)}, & 0 \le \phi_i \le \phi_c \\ 0, & \phi_i > \phi_c \end{cases} \quad (2)$$

where n denotes the corresponding refractive index. Moreover, $R_o(\varphi_i)$ in (1) is the Lambertian radiant intensity of the transmitting LEDs, which can be expressed as

$$R_o(\varphi_i) = \frac{m+1}{2\pi} \cos^m(\varphi_i) \quad (3)$$

where m is the order of Lambertian emission, which is given by

$$m = -\frac{\ln(2)}{\ln(\cos(\varphi_{1/2}))} \quad (4)$$

with $\varphi_{1/2}$ denoting the transmitter semi-angle at half power. To this effect, the receiver-site noise is drawn from a circularly-symmetric Gaussian distribution of zero mean and variance

$$\sigma_n^2 = \sigma_{sh}^2 + \sigma_{th}^2 \quad (5)$$

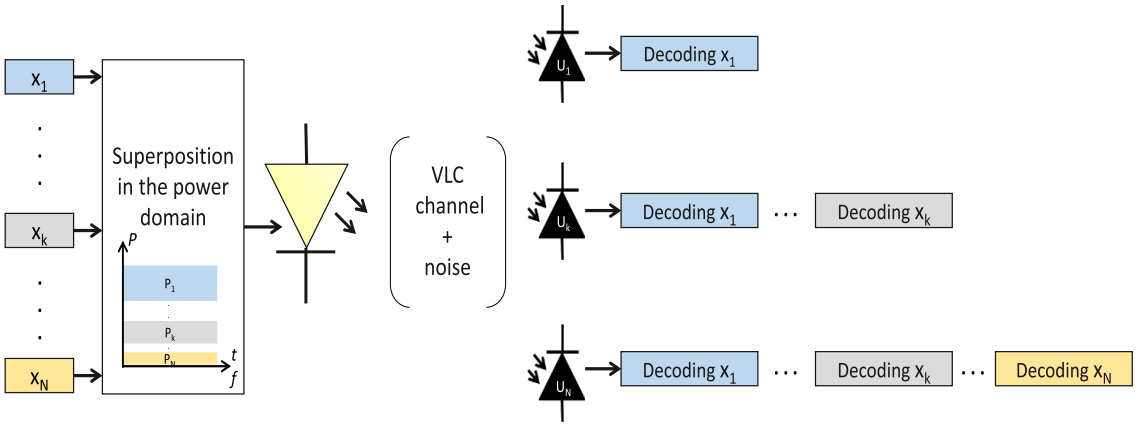

Fig. 2. NOMA-VLC downlink.

where σ_{sh}^2 and σ_{th}^2 are the variances of the shot noise and thermal noise, respectively.

The shot noise in an optical wireless channel is generated by the high rate physical photo-electronic conversion process, with variance at the i-th PD

$$\sigma_{sh_i}^2 = 2qB\left(\gamma h_i x_i + I_{bg} I_2\right) \tag{6}$$

where q is the electronic charge, γ is the detector responsivity, B is the corresponding bandwidth, I_{bg} is background current, and I_2 is the noise bandwidth factor. Furthermore, the thermal noise is generated within the transimpedance receiver circuitry and its variance is given by

$$\sigma_{th_i}^2 = \frac{8\pi K T_k}{G}\eta A I_2 B^2 + \frac{16\pi^2 K T_k \Gamma}{g_m}\eta^2 A^2 I_3 B^3 \tag{7}$$

where K is Boltzmann's constant, T_k is the absolute temperature, G is the open-loop voltage gain, A is the PD area, η is the fixed capacitance of the PD per unit area, Γ is the field-effect transistor (FET) channel noise factor, g_m is the FET transconductance, and $I_3 = 0.0868$ [39].

B. NOMA Transmission

Without loss of generality, we assume that the users $U_1, \ldots, U_N$ are sorted in an ascending order according to their channels, i.e. $h_1 \leq h_2 \leq \cdots \leq h_N$. Using NOMA, the LED transmits the real and non-negative signals $s_1, \ldots, s_N$ with associated power values $P_1, \ldots, P_N$, where s_i conveys information intended for user U_i, as shown in Fig. 2. Unless otherwise stated, the term power in the present analysis refers to the optical power which is directly proportional to the LED driving current. To this effect, the N transmitted signals are superimposed in the power domain as follows:

$$x = \sum_{i=1}^{N} P_i s_i \tag{8}$$

while the LED peak transmit power is expressed as

$$P_{\text{LED}} = \sum_{i=1}^{N} P_i. \tag{9}$$

At the PD site, direct detection of the received signal is performed based on the received optical power and the received signal at user U_k can be expressed as

$$y_k = \gamma h_k \sum_{i=1}^{N} P_i s_i + n_k \tag{10}$$

where n_k denotes zero-mean additive white Gaussian noise (AWGN) with variance σ_n^2 as given in (5). Henceforth, $\mathcal{N}(\mu, \sigma^2)$ represents the probability density function (PDF) of Gaussian distribution with mean μ and variance σ^2.

It is recalled that the multi-user interference at user U_k can be eliminated by means of SIC. Based on this, in order to decode its own signal, U_k needs to successfully decode and subtract the signals of all other users with lower decoding order, i.e. $s_1, \ldots, s_{k-1}$. As a result, the residual interference from $s_{k+1}, \ldots, s_N$ becomes insignificant and can be realistically treated as noise.

In order to facilitate SIC decoding, the LED allocates higher transmission power to users with poor channel gains. The simplest power allocation scheme is the fixed power allocation (FPA), where the associated power of the i-th sorted user is set to

$$P_i = \rho P_{i-1} \tag{11}$$

with ρ denoting the power allocation factor ($0 < \rho < 1$). According to FPA, the power allocated to user U_i is reduced at the increase of h_i because users with good channel conditions require lower power levels to successfully decode their desired signals, after canceling the interference from the signals of the users with lower decoding order. This is the fundamental principle of NOMA and has been shown to provide remarkable performance gains in RF-based communications [20].

C. SIC Detector

Using maximum-likelihood (ML) detector, the decoder at the k-th receiver decodes and subtracts the signals intended for all users U_m, where ($1 \leq m \leq k-1$). Moreover, each stage of the detection is performed with the presence of the interference from the signals of all the users with higher decoding order, i.e., $\sum_{i=m+1}^{N} P_i s_i$. As a result, the detection

threshold of the ML detector should take into account the presence of the interference terms in the received signal. Given that OOK modulation is considered, the interference caused by $s_{m+1}, \ldots, s_N$, can be expressed as $\sum_{i=k}^{2^{N-k}} \sum_{l=m+1}^{N} P_l A_{il}$, where the elements of the matrix

$$\mathbf{A} = \begin{bmatrix} A_{1\ m+1} & \cdots & A_{1\ N-1} & A_{1\ N} \\ A_{2\ m+1} & \cdots & A_{2\ N-1} & A_{2\ N} \\ A_{3\ m+1} & \cdots & A_{3\ N-1} & A_{3\ N} \\ \vdots & \vdots & \vdots & \vdots \\ A_{2^{N-m}\ m+1} & \cdots & A_{2^{N-m}\ N-1} & A_{2^{N-m}\ N} \end{bmatrix} = \begin{bmatrix} 0 & 0 & \ldots & 0 & 0 \\ 0 & 0 & \ldots & 0 & 1 \\ 0 & 0 & \ldots & 1 & 0 \\ \vdots & \vdots & \vdots & \vdots & \vdots \\ 1 & 1 & \ldots & 1 & 1 \end{bmatrix}. \tag{12}$$

demonstrate the possible combinations of interference depending on the transmitted OOK vectors. Based on this, the received signal S_m at U_k under the interference $P_l A_{il}$ follows a Gaussian distribution and its PDF can be expressed as follows:

$$\begin{cases} f_{Y_k|S_m}(y_k|s_m = 0) = \mathcal{N}_{y_k}(\gamma\, h_k P_l A_{il}, {\sigma_n}^2) \\ f_{Y_k|S_m}(y_k|s_m = 1) = \mathcal{N}_{y_k}(\gamma\, h_k (P_m + P_l A_{il}), {\sigma_n}^2). \end{cases} \tag{13}$$

As a result, we set the threshold of the ML detector to be the the mid-point between the minimum and maximum possible received signals, that is

$$\ell_{k_m} = \gamma\, h_k \frac{P_m + \sum_{l=m+1}^{N} P_l}{2}. \tag{14}$$

Hence, at each stage of SIC, U_k decides for the vector $\hat{s}_m$ that minimizes the Euclidean distance between the received signal vector y_k and the potential received signals leading to

$$\hat{s}_m = \arg\min_{s_m} \left| y_m - \ell_{k_m} \right|^2. \tag{15}$$

In what follows, we analyze the performance of NOMA based VLC systems for the standard case of perfect CSI.

III. NOMA-VLC With Perfect CSI

It is recalled that accurate CSI is of paramount importance in conventional and emerging communications as encountered imperfections in practical deployments lead to significant degradation of the overall system performance. This is also the case in VLC systems; therefore, in this section, we derive a novel analytic expression for the BER of NOMA-VLC systems employing unipolar OOK under the assumption of perfect knowledge of the channel coefficients and ideal time synchronization.

Theorem 1: Given that user U_k attempts to cancel the first $k-1$ signals from the aggregate received signal in succession, the BER of U_k achieved by the NOMA scheme can be expressed as

$$\begin{aligned} \mathrm{Pr}_{e_k} = & \sum_{e_{k-1}=-1,0,1} \cdots \sum_{e_{1}=-1,0,1} \mathcal{P}(e_{k-1}|e_1, \ldots, e_{k-2}) \\ & \times\ \mathcal{P}(e_{k-2}|e_1, \ldots, e_{k-3}) \\ & \times \cdots\ \mathcal{P}(e_1) Pr_{e_k}|e_1, \ldots, e_{k-1}. \end{aligned} \tag{16}$$

It is noted here that it can be inferred from (16) that the probability of error in decoding the k^{th} user signal depends on the detections of the signals 1 to $k-1$ that are performed during SIC stages. To this effect, the probability of error in decoding the k^{th} signal equals the conditional error probability in decoding signal k, conditioned on the error probabilities of the previous detection stages ($Pr_{e_k}|e_1, \ldots, e_{k-1}$), multiplied by the error probabilities of all the previous detection stages, where $\mathcal{P}(e_i|e_1, \ldots, e_{i-1})$ is the bit-error probability (BEP) of the i^{th} detection stage conditioned on the previous 1 to $i-1$ BEPs, which is represented as

$$\mathcal{P}(e_i|e_1, \ldots, e_{i-1}) = \begin{cases} 1 - \mathrm{Pr}_{e_i|e_1,\ldots,e_{i-1}} & e_i = 0 \\ \frac{1}{2}\mathrm{Pr}_{e_i|e_1,\ldots,e_{i-1}} & e_i = -1, 1 \end{cases}$$

with $e_i = \hat{s}_i - s_i$ denoting the error in detecting the i-th OOK signal. Also, $Pr_{e_k}|e_1, \ldots, e_{k-1}$ is the error probability in decoding the k-th signal conditioned on the previous detections, namely

$$\begin{aligned} & \mathrm{Pr}_{e_k}|e_1, \ldots, e_{k-1} \\ & = \frac{1}{2^{N-k+1}} \sum_{i=1}^{2^{N-k}} \mathcal{Q}\left(\frac{\gamma\, h_k}{\sigma_n} (\mathcal{A}_1 - \mathcal{A}_2) \right) \\ & \quad + \frac{1}{2^{N-k+1}} \sum_{i=1}^{2^{N-k}} \mathcal{Q}\left(\frac{\gamma\, h_k}{\sigma_n} (\mathcal{A}_1 + \mathcal{A}_2) \right) \end{aligned} \tag{17}$$

where

$$\mathcal{A}_1 = \frac{P_k + \sum_{l=k+1}^{N} P_l}{2} \tag{18}$$

and

$$\mathcal{A}_2 = \sum_{j=1}^{k-1} e_j P_j + \sum_{l=k+1}^{N} P_l A_{il} \tag{19}$$

with

$$\mathcal{Q}(x) \triangleq \frac{1}{\sqrt{2\pi}} \int_x^{\infty} e^{-\frac{y^2}{2}} \mathrm{d}y \tag{20}$$

denoting the one dimensional Gaussian $Q-$function. Furthermore, the term $\sum_{j=1}^{k-1} e_j P_j$ represents the potential residual interference caused by detection error in the decoding of $s_1, \ldots, s_{k-1}$ and $\sum_{l=k+1}^{N} P_l A_{il}$ corresponds to the interference caused by $s_{k+1}, \ldots, s_N$, where the elements of the matrix A in (12) demonstrate the possible combinations of interference depending on the transmitted OOK vectors.

Proof: The proof is provided in Appendix A. □

Next, we consider the realistic case of imperfect CSI.

IV. NOMA-VLC With Imperfect CSI

As already mentioned, NOMA configurations are rather sensitive to the knowledge of all users' channel coefficients. This is of paramount importance for successful data recovery at the receivers, and also crucial at the transmitter site for determining the required allocated power to each corresponding user. This is based on the fact that users must receive signals with different power levels, depending on the ordering of their channel gains, in order to effectively facilitate SIC. Thus, while the channel in VLC is technically deterministic for

specific transmitter-receiver specifications and fixed locations, the assumption of perfect CSI is not practically realistic even for indoor VLC systems. It is also noted that, typically, CSI can be firstly determined at the receiver site with the aid of periodic pilot signals and then, the receivers feed back the quantized channel coefficients to the transmitters through an RF or infrared (IR) uplink.[1] To this effect, the uncertainty in the VLC channel estimation arises from the noise in the downlink and uplink channels as well as from the mobility of users in indoor environments. Moreover, AD/DA conversion of the channel estimates introduces quantization errors that add to the channel uncertainty[2] [40]. Based on this, it becomes evident that it is essential to quantify the effects of imperfect CSI on the performance of NOMA VLC systems. To this end, we consider two different realistic stochastic uncertainty models for the CSI, namely noisy CSI and outdated CSI.

A. Noisy CSI

By assuming that $\hat{h}_k$ is the estimate for the channel between the k-th user and the transmitting LED, it follows that

$$\hat{h}_k = h_k + \epsilon_n \tag{21}$$

where ϵ_n denotes the channel estimation error modeled as a zero-mean Gaussian distribution with variance $\sigma^2_{\epsilon_n}$, i.e, $\epsilon_n \sim \mathcal{N}(0, \sigma^2_{\epsilon_n})$, which has been adopted as a reasonable model for indoor VLC systems [30], [32]. To this effect, it immediately follows that the channel estimate $\hat{h}_k$ can be modeled as $\hat{h}_k \sim \mathcal{N}(h_k, \sigma^2_{\epsilon_n})$. Under the realistic case of noisy CSI, the conditional error probability for user U_k can be approximated by the following Proposition.

Proposition 1: Under noisy CSI, the error of decoding the k*-th signal at U_k conditioned on the previous detections is given by*

$$\begin{aligned}\Pr_{e_k}|e_1,\ldots,e_{k-1} &\approx \frac{\sqrt{2}}{2^{N-k+1}\sigma_{\epsilon_n}} \sum_{i=1}^{2^{N-k}} \frac{e^{c-\frac{\gamma\left(8\ a\gamma \mathcal{S}_k{}^2 h^2 + b\mathcal{A}_3\right)}{4\ a\gamma^2 \mathcal{P}_k{}^2 \sigma_{\epsilon_n}{}^2 - 8\sigma_n{}^2}}}{\sqrt{\alpha_i}} \\ &+ \frac{\sqrt{2}}{2^{N-k+1}\sigma_{\epsilon_n}} \sum_{i=1}^{2^{N-k}} \frac{e^{c-\frac{\gamma\left(8\ a\gamma \hat{\mathcal{S}}_k h^2 + b\mathcal{A}_3\right)}{4\ a\gamma^2 \mathcal{P}_k{}^2 \sigma_{\epsilon_n}{}^2 - 8\sigma_n{}^2}}}{\sqrt{\hat{\alpha}_i}}\end{aligned} \tag{22}$$

where

$$\mathcal{A}_3 = \gamma\, b \mathcal{P}_k{}^2 \sigma_{\epsilon_n}{}^2 + 8h\mathcal{P}_k\sigma_n \tag{23}$$

with

$$\mathcal{P}_k = P_k + \sum_{l=k+1}^{N} P_l \tag{24}$$

and

$$\hat{\alpha} = \frac{2}{\sigma_{\epsilon_n}{}^2} - \frac{a\gamma^2 S_k^s}{\sigma_n{}^2} \tag{25}$$

[1]Although VLC uplink can be theoretically possible, it is practically energy-inefficient for low-power mobile devices. Thus, utilizing uplink-downlink reciprocity for acquiring CSI at the transmitter is not technically relevant in the context of VLC systems.

[2]This topic is beyond the scope of the present work.

while the terms $\mathcal{S}_k$ and $\hat{\mathcal{S}}_k$ are given by

$$\mathcal{S}_k = \frac{\mathcal{P}_k}{2} + \sum_{j=1}^{k-1} e_j P_j + \sum_{l=k+1}^{N} P_l A_{il} \tag{26}$$

and

$$\hat{\mathcal{S}}_k = \frac{\mathcal{P}_k}{2} - \sum_{j=1}^{k-1} e_j P_j - \sum_{l=k+1}^{N} P_l A_{il} \tag{27}$$

respectively.

Proof: The proof is provided in Appendix B. □

B. Outdated CSI

Outdated CSI error may result from the variations in channel realizations due to the mobility of users and/or shadowing effects that occur after the latest channel estimate update. In this context, we consider a deterministically bounded random variable ϵ_o to model the outdated CSI error as

$$\hat{h}_k = h_k + \epsilon_o \tag{28}$$

where $\epsilon_o \leq \mathcal{E}$, with $\mathcal{E}$ denoting the error bound that occurs when the mobile user moves with maximum velocity between the reception of pilot signals and data [32]. In what follows, we derive a tight upper bound for the conditional error probability at user U_k.

Proposition 2: The conditional error probability at user U_k for the case of outdated CSI can be upper bounded as follows:

$$\begin{aligned}&\Pr_{e_k}|e_1,\ldots,e_{k-1} \\ &\leq \frac{2^k}{2^{N+1}} \sum_{i=1}^{2^{N-k}} \mathcal{Q}\left(\mathcal{A}_4 - \frac{\gamma h_k}{\sigma_n}\mathcal{A}_2\right) \\ &\quad + \frac{2^k}{2^{N+1}} \sum_{i=1}^{2^{N-k}} \mathcal{Q}\left(\frac{\gamma h_k}{\sigma_n}(P_k + \mathcal{A}_2) - \mathcal{A}_4\right)\end{aligned} \tag{29}$$

where

$$\mathcal{A}_4 = \frac{\mathcal{P}_k}{2\sigma_n}\mathcal{E} + \frac{\gamma h_k}{\sigma_n}\frac{\mathcal{P}_k}{2} \tag{30}$$

and

$$\mathcal{P}_k = P_k + \sum_{l=k+1}^{N} P_l. \tag{31}$$

Proof: The proof is provided in Appendix C. □

Determination of the Value of $\mathcal{E}$: In order to obtain the upper bound on the CSI error, we simplify the channel gain by inserting (2) and (3) into (1) and substituting $\cos\varphi_i$ with z/d_i, where z denotes the height between the LEDs and the PDs, which is assumed to be fixed, i.e., at a level of an ordinary table. Based on this and by assuming vertical alignment of LEDs and PDs, the corresponding channel gain h_i can be expressed as

$$h_i = \frac{\varpi}{d_i^{m+3}} \tag{32}$$

where

$$\varpi = \frac{(m+1)A_i T_s(\phi_i) g(\phi_i)}{2\pi}. \tag{33}$$

By now referring to Fig. 3, let user U_k move along the horizontal plane from (x_1, y_1) to (x_2, y_2) with maximum

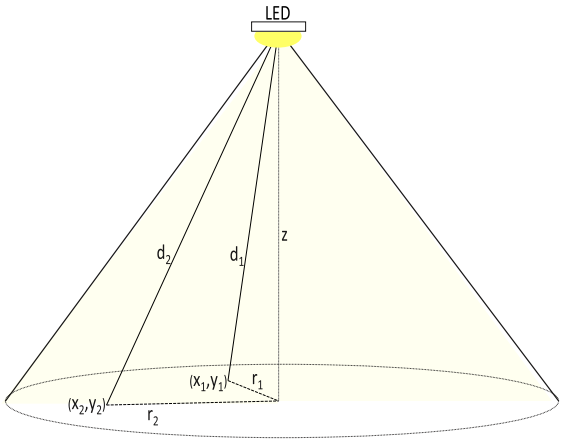

Fig. 3. Outdated CSI resulting from user mobility.

velocity υ. Then, the error bound $\mathcal{E}$ can be calculated as follows:

$$\mathcal{E} = \varpi |d_2^{m+3} - d_1^{m+3}| \tag{34}$$

where

$$d_1^2 = r_1^2 + z^2, \tag{35}$$

$$d_2^2 = r_2^2 + z^2 \tag{36}$$

and

$$\sqrt{((x_1 - x_2)^2 + (y_1 - y_2)^2)}\,\mathrm{t} \tag{37}$$

with t denoting the time elapsed since the last CSI update. It is evident that the algebraic representation of (34) is tractable and can be computed straightforwardly. Furthermore, it is particularly accurate, as shown in detail in Section VI.

V. NOMA-VLC With Dimming Control

In this Section, we investigate the performance of NOMA-VLC under dimming control. To this end, it is firstly recalled that adjusting the brightness level of the LED can be achieved by two approaches: 1) analog dimming, where the driving current of the LED is directly adjusted to the required illumination level; 2) digital dimming, in which the driving current is maintained constant while the duty cycle is varied in order to acquire the desired brightness [41], [42]. Therefore, analog dimming is straightforward to implement given that the LED brightness is directly proportional to the forward current. However, this technique may cause chromaticity shift problems as it alters the transmitted wavelength. To implement analog dimming, we use unipolar OOK signal to drive the LED and dimming is achieved by altering the driving current to match the dimming target. In this context, the driving current, and, consequently, the transmitted optical power, are set to be proportional to the dimming factor γ_d. In this case, the error in decoding the k-th signal conditioned on the previous detections can be obtained by (17), (22) and (29) for perfect, noisy and outdated CSI, respectively by changing the transmit power from P to $\gamma_d P$.

On the contrary, digital dimming imposes a pulse width modulation (PWM) signal with a duty cycle that is determined by the required dimming factor. This technique alleviates the chromaticity shifts, but at a cost of reduced spectral efficiency. In the present analysis, we implement digital dimming by means of VOOK as in [35], where the brightness of the LED is controlled by adopting the data duty cycle δ_d of the OOK signal. Based on this, information bits are transmitted when the duty cycle is on, while the off portion is filled with dummy bits that are either zeros or ones, depending on the dimming factor γ_d. VOOK codewords are depicted in Table I, indicating that when $\gamma_d = 0$, the lights are completely turned off while when $\gamma_d = 1$, full brightness is achieved. Accordingly, no data bits are transmitted when γ_d is set to 0 or 1. We consider the special case when the data bits in a single codeword are redundant. i.e., repetition coding is implied. It is noted here that digital dimming can also be performed with different transmitted data bits in a single codeword. To this effect, with the use of coded VOOK, the BER in decoding the k-th signal conditioned on the previous k-1 detections can be expressed as follows

TABLE I
VOOK Codewords

γ_d	δ_d	**VOOK Codeword**
1.0	1.0	1111111111
0.9	0.2	dd11111111
0.8	0.4	dddd111111
0.7	0.6	dddddd1111
0.6	0.8	ddddddd11
0.5	1.0	dddddddddd
0.4	0.8	ddddddd00
0.3	0.6	dddddd0000
0.2	0.4	dddd000000
0.1	0.2	dd00000000
0.0	0.0	0000000000

$$\Pr_{e_k VOOK}|e_1, \ldots, e_{k-1} = \sum_{\lceil i=n/2 \rceil}^{n} \binom{n}{i} \Pr^{i}_{e_k|e_1,\ldots,e_{k-1}} \times (1 - \Pr_{e_k|e_1,\ldots,e_{k-1}})^{n-i} \tag{38}$$

where $\Pr_{e_k|e_1,\ldots,e_{k-1}}$ can be obtained from (17), (22) and (29) for perfect, noisy and outdated CSI respectively, whereas n is the number of redundant bits in the VOOK codewords, calculated as

$$n = \begin{cases} 20\gamma_d, & 0 < \gamma_d \leq \frac{1}{2} \\ 20 - 20\gamma_d, & \frac{1}{2}\gamma_d < 1. \end{cases} \tag{39}$$

It is noted here that the value of γ_d for both analog and digital dimming indicates the same brightness levels. For example, when $\gamma_d = 0.8$, in the case of analog dimming, the driving current will be multipled by 0.8, so the transmitted optical power will be 80% of the peak power. A digital dimming of $\gamma_d = 0.8$ indicates a duty cycle of 0.4; so 4 bits out of 10 will be data bits with an average power of 2 ones and 2 zeros (as the 0's and 1's are equiprobable), while the remaining 6 bits will be filled with 1's. This is equivalent to an average transmit power that is 80% of the peak power. Finally, it is also noted that the use of redundant bits in VOOK leads

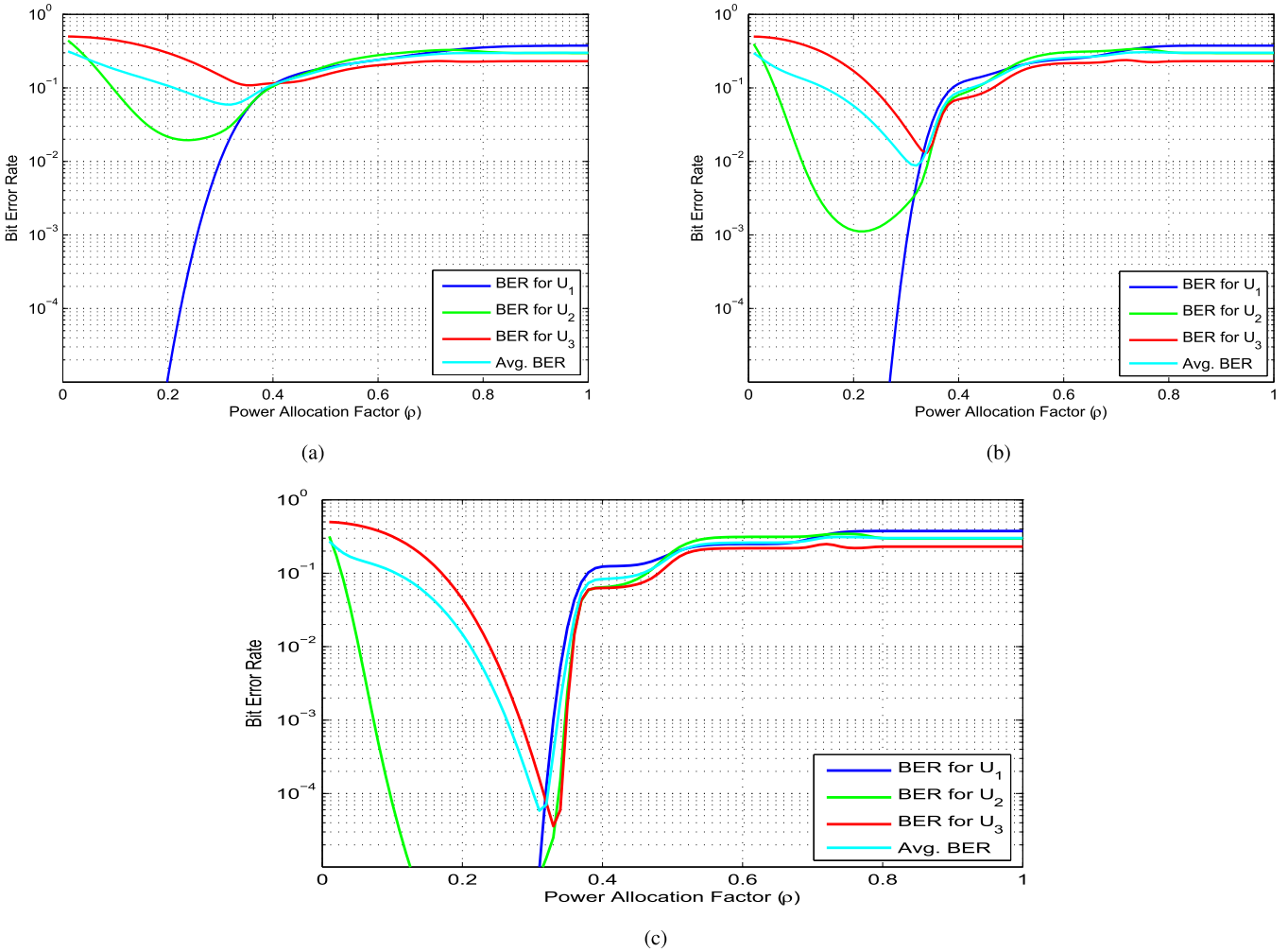

Fig. 4. BER performance under fixed power allocation: (a) SNR=110 dB, (b) SNR=115 dB and (c) SNR=120 dB.

to BER improvements as n increases; yet, digital dimming also affects the system spectral efficiency as the achievable data rate deteriorates linearly with the number of bits in the corresponding codewords.

VI. Numerical Results and Discussion

In this section, we employ the derived analytic expressions in the analysis of the considered setups. Respective results from extensive Monte Carlo simulations are also provided to verify the validity and usefulness of the offered results. Thus, the BER performance of a NOMA-VLC downlink system is analyzed for different scenarios based on the system and channel models in Section II. It should be noted here that the considered channel model is independent of the room geometry. However, the room dimensions are needed so that the locations of users are generated within the room boundaries for the simulation results involving mobility. Based on this and without loss of generality, we consider that the users exist within a typical room of dimensions $4m \times 4m \times 3m = 48m^3$, which corresponds to a realistic indoor environment.

We consider one transmitting LED mounted at the center of the ceiling and, in order to ensure fair comparability, fixed LED transmitting power is used in all scenarios. We also assume the existence of three users in the coverage area of the transmitting LED that are planned to be served simultaneously using NOMA. It is emphasized here that this number of users is selected for indicative purposes and that the considered system model is generic and applicable to any number of users. In this context, the LED superimposes the signals of the three users in the power domain by allocating the power values P_1, P_2 and P_3 to U_1, U_2 and U_3 respectively, under the constraint $P_1 + P_2 + P_3 = P_{\text{LED}}$. In the used notation, U_i denotes the user in i-th decoding order; that is, h_i is in the i-th ascending order of the channel gains. The used simulation parameters are shown in Table II, while the channel gains and coordinates of all users are depicted in Table III. For the results that involve users' mobility, the locations of the users are randomly generated. It should be noted here that the underlying symmetry in VLC systems may lead to similar channel gains and, consequently, resulting in a higher error rate. This issue was addressed in an earlier work [18], where a strategy was proposed based on tuning the FOVs of the receiving PDs in order to maximize the differences between the channel gains and improve the performance of NOMA.

Next, we evaluate the BER performance with regard to the transmit SNR in order to include the individual path gain of each user. Since the channel gain is in the order of 10^{-4}, the corresponding results exhibit an offset of about 80 dB with

TABLE II
SIMULATION PARAMETERS

Description	Notation	Value	Description	Notation	Value
LED power	P_{LED}	0.25 W	open-loop voltage gain	G	10
transmitter semi-angle	φ_i	50 deg	fixed capacitance	η	112 pF/cm2
FOV of the PDs	ϕ_{c_i}	45 deg	FET channel noise factor	Γ	1.5
physical area of PD	A_i	1.0 cm^2	FET transconductance	g_m	30 mS
refractive index	n	1.5	absolute temperature	T_k	298 K
gain of optical filter	$T_s(\phi_{li})$	1.0	responsivity	γ	1 A/W
bandwidth	B	10 Mbps	noise bandwidth factors	I_2	0.562
noise bandwidth factors	I_3	0.0868	background current	I_{bg}	5100 μA

TABLE III
USERS SETUP

User	Coordinates	FOV	Channel Gain
U_1	(2.5,2.5,1.25)	60	0.2835×10^{-4}
U_2	(2.4,2.4,1.25)	45	0.4787×10^{-4}
U_3	(2.3,2.3,1.25)	45	0.5272×10^{-4}

respect to the SNR at the receiver site. First, we investigate the effect of the power allocation factor ρ in (11) on the BER performance under fixed power allocation. To this end, Fig. 4 shows the average BER and the individual BER for the three users versus ρ for different transmit SNR values of 110 dB, 115 dB and 120 dB. It is shown that, despite its poor channel conditions, the user in the first decoding order, i.e., U_1, experiences comparable error performance to other users. This is because the signal intended for this user is transmitted with a high power compared to other signals in order to enable U_1 to directly decode its signal of interest regardless of the interference it receives. Moreover, the best average BER performance for all users can be achieved at about $\rho = 0.3$, as in this value, the power levels allocated to users experiencing low channel gains are sufficiently high to enable correct signal decoding. As ρ increases, users with favorable channel conditions receive with higher power levels, which in turn reduces the power associated with the signals of the other users. As a consequence, errors occur in the early stages of SIC decoding, and are then inherited by the following stages, which ultimately leads to poor BER performance. It is noted here that $\rho = 0.3$ is considered in the following results of this Section.

The BER expression derived in Section III is validated by Fig. 5, which illustrates the BER performance of the three users assuming perfect CSI. It is shown that the derived analytic results are in excellent agreement with the respective Monte Carlo simulation results. It is evident that the user with the lowest decoding order exhibits the best BER performance, while the performance degrades as the decoding order increases. Yet, all users exhibit satisfactory performance above transmit SNR of 120 dB that corresponds to a receive SNR of about 40 dB, which is a typical range in VLC transmissions.

Next, we investigate the effect of channel uncertainty on the performance of NOMA-VLC. To this end, we assume that the uplink to the LED is error free, so that the LED

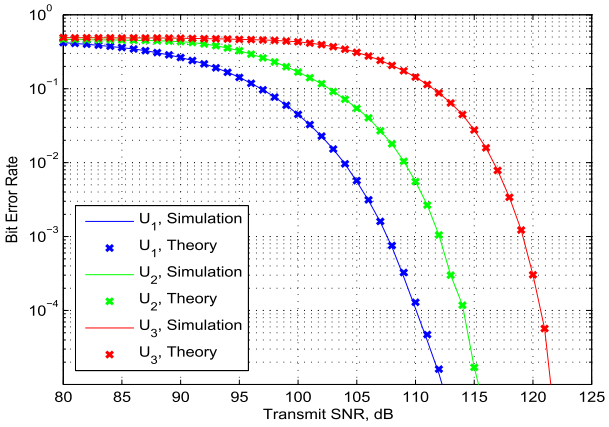

Fig. 5. BER Performance with Perfect CSI.

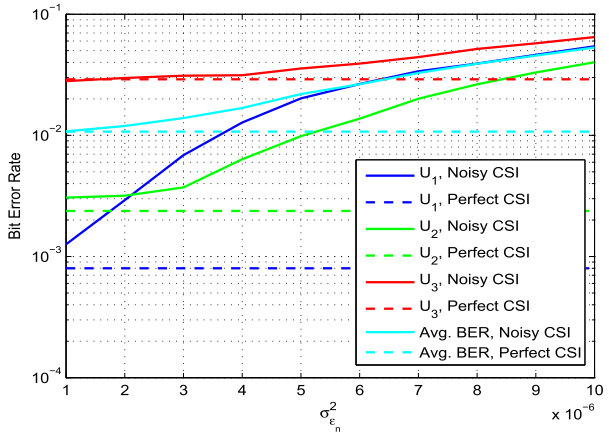

Fig. 6. BER Performance for different values of $\sigma^2_{\epsilon_n}$.

and the users have the same estimates of the channel gains.[3] For the case of noisy CSI, two different models are used: 1) fixed error variance, where $\sigma^2_{\epsilon_n}$ is independent of the transmit SNR; 2) varying error variance, where $\sigma^2_{\epsilon_n}$ is a decreasing function of the transmit SNR. Furthermore, we assume that the noisy channel error variances are identical at the different users. In order to obtain an insight into the impact of different CSI variances on the system performance, Fig. 6 illustrates the BER performance versus different fixed values of $\sigma^2_{\epsilon_n}$

[3]This is a valid assumption for an RF uplink that has been commonly adopted in the technical literature [43], [44].

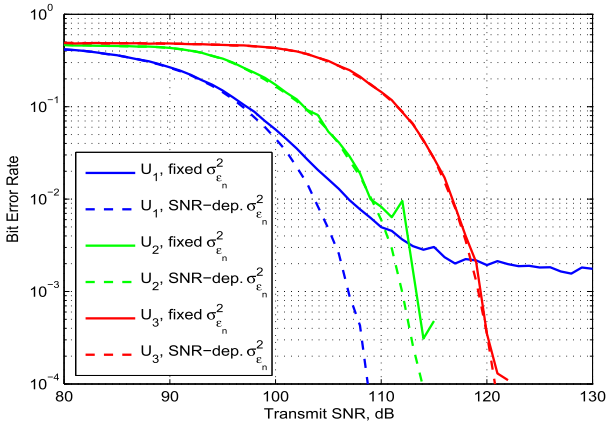

Fig. 7. BER Performance with Noisy CSI, for fixed and SNR-dependent error variances.

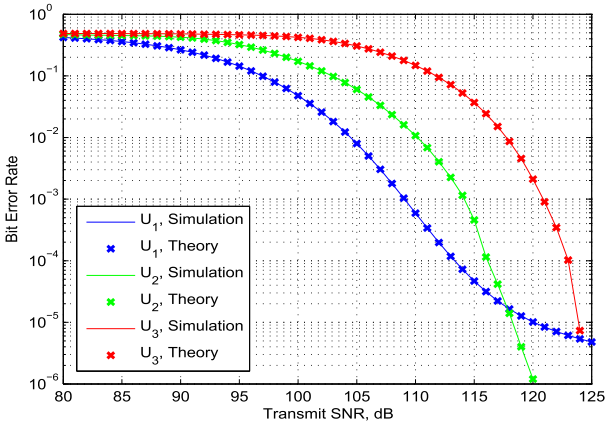

Fig. 8. BER Performance with Noisy CSI, $\sigma^2_{\epsilon_n} = 2 \times 10^{-6}$.

at a transmit SNR of 115 dB. It is clear that users with lower decoding order suffer from higher errors due to the involved channel uncertainty. This is particularly evident at user U_1, which exhibits substantial BER degradation compared to the error-free CSI (indicated by dashed line). The reason is that U_1 has the lowest channel gain among all users, which renders signal detection highly sensitive to errors in the available CSI. Moreover, U_1 is expected to decode x_1 with the existence of high interference from the signals of other users, which increases the severity of the effect of imperfect CSI. Furthermore, although other users also need to decode x_1 despite the involved interference, their relatively high channel gains make the detection more robust to channel errors from the early stages of the detection. This is specifically clear for U_3, which is the least affected by channel uncertainty. It is noted here that the CSI error resulting from the noisy channel is in general small enough to avoid affecting the ordering of channel gains. Hence, the power allocation based on CSI available at the transmitter is not ultimately affected. Fig. 7 demonstrates the corresponding BER performance under fixed and SNR-dependant error variances. It is observed that fixed $\sigma^2_{\epsilon_n}$ results in an irreducible error floor at high SNRs for users with low decoding order. However, when $\sigma^2_{\epsilon_n}$ is modeled as SNR-dependant, the BER decreases with the increase in transmit SNR. It is not surprising to observe that the performance of user U_3 is almost the same for the two variance models, which is due to the fact that the impact of error is already insignificant at this user. In order to validate the BER expression for noisy CSI in *Proposition 1*, we demonstrate the BER performance using the derived approximation along with respective results from Monte Carlo simulations in Fig. 8. It is observed that, the derived approximation provides accurate results that are in tight agreement with the simulation results. Moreover, it is noted that the user in the first decoding order experiences higher performance degradation compared to users with higher decoding orders. This is due to the fact that U_1 does not perform SIC, which means that it has to deal with the existing interference along with the CSI error. Moreover, U_1 has the lowest channel gain among all users, which makes the effect of noisy CSI particularly detrimental.

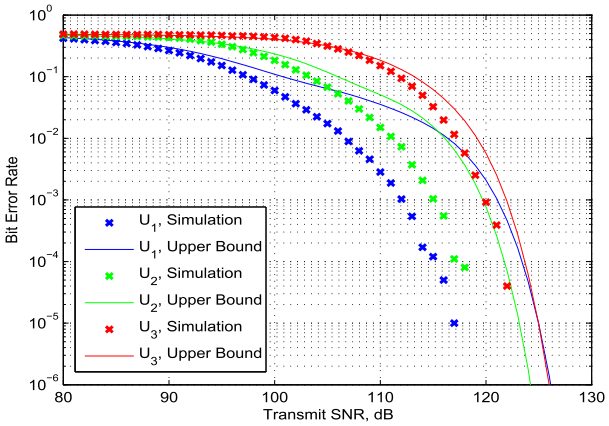

Fig. 9. BER Performance with Outdated CSI and unaltered order.

We also quantify the effects by the mobility of the indoor users. To this end, it is recalled that VLC channels are mainly dependent upon the user location with respect to the transmitting LED. As a consequence, even a slight change in the user's location results in a change of the corresponding channel gain. To this effect, if a user possesses an outdated channel estimation, i.e., a change of location occurs before the next channel update, CSI becomes erroneous. In order to quantify the impact of outdated CSI on the overall system performance, we simulate the mobility of indoor users with random speed from 0 to 2 m/s while they remain connected to the same LED. We then assume that the change in location may occur between CSI updates and thus, both the transmitter and the receiver come to use the outdated CSI for power allocation and decoding, respectively. It is also noted here that outdated CSI, unlike noisy CSI, may lead to a change in the ordering of the channel gains of the users, which ultimately leads to unfair power allocation at the transmitter, where high power values may be allocated to users with good channel conditions and vice versa. This results in a dramatic performance degradation for users with poor channel gains, as their allocated power becomes insufficient for successful decoding. In the same context, Fig. 9 and Fig. 10 demonstrate the BER performance with outdated CSI for the three users,

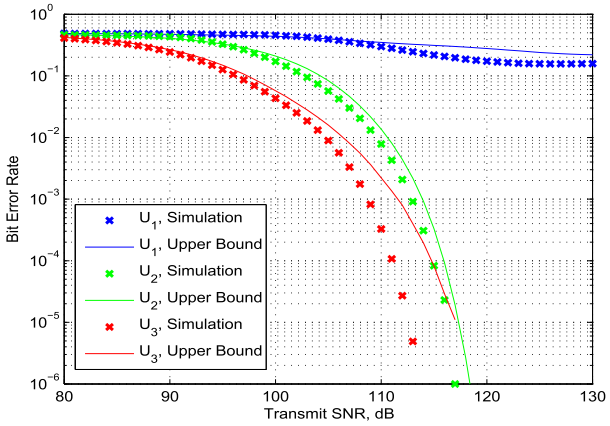

Fig. 10. BER Performance with Outdated CSI and altered order.

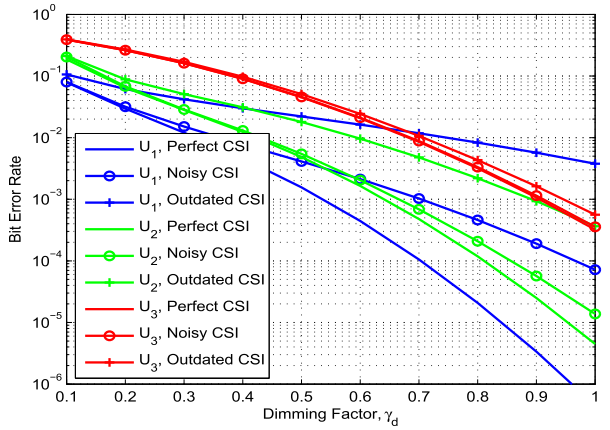

Fig. 11. BER Performance with analog intensity dimming.

where the upper bound for the error is determined by (29), in *Proposition 2*, when the user moves with maximum velocity. In Fig. 9, we simulate the mobility of users assuming that their relative channel ordering remains constant, which is valid if users change locations in the same trend, i.e. Reference Point Group Model [45], which is realistic in large indoor environments, such as museums or airports. On the contrary, Fig. 10 illustrates the performance degradation caused by unfair power allocation when outdated CSI leads to change in the ordering of users' gains. It is noted that for the sake of consistency with other figures, U_1 here denotes the user that has the lowest channel gain among all users. However, U_1 is now not in the first decoding order as its channel is erroneously estimated not to be the lowest. Therefore, users with low channel gains suffer, as expected, from dramatic degradation, while U_3 benefits from the high power that is in fact erroneously allocated to it. As a consequence, the high power allows U_3 to detect the desired signal effectively, even though the estimate of h available at the decoder is practically inaccurate.

Finally, we evaluate the BER performance of the NOMA-VLC system under dimming control. Fig. 11 and Fig. 12 demonstrate the BER of the three users under analog and digital dimming schemes, respectively. As expected, analog intensity dimming leads to BER

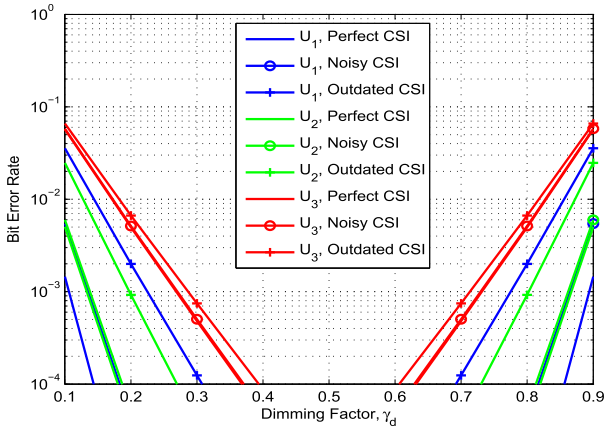

Fig. 12. BER Performance with digital VOOK dimming.

performance degradation, particularly at low γ_d values, as lower transmit power is used, which reduces the received SNR. On the contrary, digital dimming employed by means of VOOK leads to BER enhancement, that is substantial when the dimming factor is around 0.5. This is achieved thanks to the increase of redundant data bits, which in turn reduces the probability of incorrect detections. Yet, this enhancement comes at the cost of reduction in the achievable throughput, which is the main drive for NOMA. The effect of imperfect CSI under dimming is also demonstrated, indicating that outdated CSI leads to higher performance degradation compared to noisy CSI, which is in agreement with the previous results.

VII. Conclusions

This work was devoted to the analysis of the BER performance in a downlink VLC network where multiple access was provided by means of NOMA. This was realized for the case of both perfect and imperfect CSI, which showed that noisy CSI leads to, as expected, a degradation of the system performance. However, this degradation is rather smaller compared to the one created by outdated CSI, which results from the mobility of the user terminal between two CSI updates. It was shown that this leads to considerable performance degradation if the ordering of the users' channel gains changes between the channel updates. The validity of the derived analytic results was justified by extensive comparisons with results from respective Monte Carlo simulations. Finally, the offered results led to meaningful theoretical and practical insights that are expected to be useful in realistic design and future deployments of VLC systems.

Appendix A
Proof of Theorem 1

Using ML detector, the decoder at the k-th receiver decides for $\hat{s}$ that minimizes the Euclidean distance between the received signal y and the potential received signals leading to

$$\hat{s} = \arg\min_{s} |y - \gamma\, h_k s|^2 . \tag{40}$$

Based on this and assuming that the U_k user cancels successfully the signals $s_1, \ldots, s_{m-1}$, the error probability at U_k in detecting the signal s_m intended to user U_m $(1 \leq m \leq k-1)$

can be expressed according to the state of the transmitted symbol, s_m. Specifically, when the transmitted symbol $s_m = 0$, the conditional error probability is given by

$$\Pr_{e_{m\to k|s_m=0}} = \int_{\ell_{k_m}}^{\infty} \mathcal{N}_{y_k}\left(\gamma\, h_k \sum_{i=m+1}^{N} P_i s_i, \sigma_n\right) \mathrm{d}y_k \tag{41}$$

which can be expressed in closed-form in terms of the $Q-$function, namely

$$\Pr_{e_{m\to k|s_m=0}} = Q\left(\frac{\gamma\, h_k}{\sigma_n}\left(\frac{P_m + \sum_{l=m+1}^{N} P_l}{2} - \mathcal{A}_5\right)\right) \tag{42}$$

where

$$\mathcal{A}_5 = \sum_{i=m+1}^{N} P_i s_i. \tag{43}$$

On the contrary, when $s_m = 1$ is transmitted, it follows that

$$\Pr_{e_{m\to k|s_m=1}} = \int_{-\infty}^{\ell_{k_m}} \mathcal{N}_{y_k}\left(\gamma\, h_k \left(P_m + \mathcal{A}_5\right), \sigma_n\right) \mathrm{d}y_k \tag{44}$$

which after some algebraic manipulations, it can be explicitly expressed as follows:

$$\Pr_{e_{m\to k|s_m=1}} = 1 - Q\left(\frac{\gamma\, h_k}{\sigma_n}\left(-\frac{P_m + \sum_{l=m+1}^{N} P_l}{2} - \mathcal{A}_5\right)\right) \tag{45}$$

which with the aid of the identity $Q(-x) \triangleq 1 - Q(x)$, it can be equivalently re-written as

$$\Pr_{e_{m\to k|s_m=1}} = Q\left(\frac{\gamma\, h_k}{\sigma_n}\left(\frac{P_m + \sum_{l=m+1}^{N} P_l}{2} + \mathcal{A}_5\right)\right). \tag{46}$$

It is noted that the above expressions assume perfect cancellation of the first $m-1$ signals. Nevertheless, detection errors may practically occur in any step of the successive cancellation process. Therefore, considering the contribution of the residual interference inherited by cancellation errors, equations (42)-(44) can be alternatively re-written as

$$\begin{aligned}\Pr_{e_{m\to k|s_m=0}} &= \int_{\ell_{k_m}}^{\infty} \mathcal{N}_{y_k}\left(\gamma\, h_k \left(\mathcal{A}_6 + \mathcal{A}_5\right), \sigma_n\right) \mathrm{d}y_k \\ &= Q\left(\frac{\gamma\, h_k}{\sigma_n}\left(\frac{P_m + \sum_{l=m+1}^{N} P_l}{2} - \mathcal{A}_6 - \mathcal{A}_5\right)\right)\end{aligned} \tag{47}$$

and

$$\begin{aligned}\Pr_{e_{m\to k|s_m=1}} &= \int_{-\infty}^{\ell_{k_m}} \mathcal{N}_{y_k}\left(\gamma\, h_k \left(P_m + \mathcal{A}_6 + \mathcal{A}_5\right), \sigma_n\right) \mathrm{d}y_k \\ &= Q\left(\frac{\gamma\, h_k}{\sigma_n}\left(\frac{P_m + \sum_{l=m+1}^{N} P_l}{2} + \mathcal{A}_6 + \mathcal{A}_5\right)\right)\end{aligned} \tag{48}$$

respectively, where

$$\mathcal{A}_6 = \sum_{j=1}^{m-1} e_j P_j. \tag{49}$$

APPENDIX B
PROOF OF PROPOSITION 1

According to (21), the ML decision rule at user U_k is readily expressed as

$$\hat{s} = \arg\min_{s} \left| y - \gamma\, \hat{h}_k s \right|^2. \tag{50}$$

To this effect, the error probability at U_k in detecting the signal s_m intended to user U_m $(1 \le m \le k-1)$ can be represented as follows:

$$\Pr_{e_{m\to k|s_k=0}} = \int_{\hat{\ell}_{k_m}}^{\infty} \mathcal{N}_{y_k}\left(\gamma\, h_k \left(\mathcal{A}_6 + \mathcal{A}_5\right), \sigma_n\right) \mathrm{d}y_k \tag{51}$$

and

$$\Pr_{e_{m\to k|s_k=1}} = \int_{-\infty}^{\hat{\ell}_{k_m}} \mathcal{N}_{y_k}\left(\gamma\, h_k \left(P_m + \mathcal{A}_6 + \mathcal{A}_5\right), \sigma_n\right) \mathrm{d}y_k \tag{52}$$

where $e_j = \hat{s}_j - s_j$, and

$$\hat{\ell}_{k_m} = \gamma\, \hat{h}_k \frac{P_m + \sum_{l=m+1}^{N} P_l}{2}. \tag{53}$$

Based on this, and after some algebraic manipulations, the conditional error probability in (17) becomes

$$\begin{aligned}\Pr_{e_k|e_1,\ldots,e_{k-1}} &= \frac{1}{2^{N-k+1}} \\ &\times \int_{-\infty}^{\infty} \left\{ \sum_{i=1}^{2^{N-k}} Q\left(\frac{\gamma\, \epsilon_n \mathcal{A}_7}{\sigma_n} + \frac{\gamma\, h_k}{\sigma_n}\left(\mathcal{A}_7 - \mathcal{A}_2\right)\right) \right. \\ &\left. + \sum_{i=1}^{2^{N-k}} Q\left(\frac{\gamma\, h_k}{\sigma_n}\left(\mathcal{A}_7 + \mathcal{A}_2\right) - \frac{\gamma\, \epsilon_n \mathcal{A}_7}{\sigma_n}\right) \right\} \mathcal{N}_{\epsilon_n}\left(0, \sigma_{\epsilon_n}^2\right) \mathrm{d}h_k\end{aligned} \tag{54}$$

where

$$\mathcal{A}_7 = \frac{P_k + \sum_{l=m+1}^{N} P_l}{2}. \tag{55}$$

It is evident that the derivation of an exact closed-form expression to (54) is subject to analytic evaluation of the involved two integrals. However, this is unfortunately not feasible as these integrals are not available in the open technical literature. Yet, a relatively simple closed-form approximation can be derived instead, which appears to be particularly accurate for all values of the considered scenario. To this end, it is recalled that the one dimensional Gaussian Q-function can be accurately expressed by a tight approximation in [46], namely

$$Q(x) \approx e^{ax^2+bx+c}, \quad x \ge 0 \tag{56}$$

where $a, b, c \in \mathbb{R}$ are the corresponding fitting parameters that are selected to maximize the sum of square errors (SSE), over the range $\hat{x} \in [0, 20]$. Following [46], the values that have been used are $a = -0.3842$, $b = -0.7640$ and $c = -0.6964$. This leads to highly accurate results as this approximation of the $Q-$functions is particularly accurate and has been used extensively in the literature. These values are available in [46] and ensure increased tightness as the corresponding involved absolute and relative errors between the exact and approximated values are particularly small for the entire range

of values of x. To this effect, by performing the necessary variable transformation in (56) and substituting in (54), one obtains the closed-form expression in (22), which completes the proof.

APPENDIX C
PROOF OF PROPOSITION 2

Using ML detection, it follows that

$$\Pr_{e_{m\to k|s_k=0}} = \int_{\hat{\ell}_{k_m}}^{\infty} \mathcal{N}_{y_k}\left(\gamma\, h_k\left(\mathcal{A}_6+\mathcal{A}_5\right),\sigma_n\right)\mathrm{d}y_k. \tag{57}$$

The above integral representation can be also expressed in closed-form in terms of the $Q-$function. Based on this, it immediately follows that

$$\Pr_{e_{m\to k|s_k=0}} = Q\left(\gamma\,\hat{h}_k\frac{P_m+\sum_{l=m+1}^{N}P_l}{2\sigma_n}-\mathcal{A}_8(\mathcal{A}_6+\mathcal{A}_5)\right) \tag{58}$$

where

$$\mathcal{A}_8 = \frac{\gamma\, h_k}{\sigma_n} \tag{59}$$

which can be equivalently expressed as

$$\Pr_{e_{m\to k|s_k=0}} = Q\left(\frac{\gamma\, P_m+\sum_{l=m+1}^{N}P_l}{2\sigma_n\mathcal{E}^{-1}}+\frac{\mathcal{A}_8 P_m}{2}-\mathcal{A}_8\mathcal{A}_2\right). \tag{60}$$

Likewise,

$$\Pr_{e_{m\to k|s_k=1}} = \int_{-\infty}^{\hat{\ell}_{k_m}} \mathcal{N}_{y_k}\left(\gamma\, h_k\left(P_m+\mathcal{A}_6+\mathcal{A}_5\right),\sigma_n\right)\mathrm{d}y_k \tag{61}$$

which can be expressed in closed-form as

$$\Pr_{e_{m\to k|s_k=1}} = 1-Q\left(\gamma\,\hat{h}_k\frac{\mathcal{A}_9}{2\sigma_n}-(P_m+\mathcal{A}_6+\mathcal{A}_5)\mathcal{A}_8\right) \tag{62}$$

and

$$\Pr_{e_{m\to k|s_k=1}} = Q\left(-\frac{\gamma\, P_m+\sum_{l=m+1}^{N}P_l}{2\sigma_n}\mathcal{E}+\frac{\gamma\, h_k}{\sigma_n}\mathcal{A}_{10}\right) \tag{63}$$

where

$$\mathcal{A}_9 = P_m+\sum_{l=m+1}^{N}P_l \tag{64}$$

and

$$\mathcal{A}_{10} = \frac{P_m-\sum_{l=m+1}^{N}P_l}{2}+\sum_{j=1}^{m-1}e_j P_j+\sum_{l=m+1}^{N}P_l A_{il} \tag{65}$$

with $e_j = \hat{s_j}-s_j$. Based on this and after carrying out some algebraic manipulations, equation (29) is deduced, which completes the proof.

ACKNOWLEDGMENTS

The authors wish to thank the anonymous reviewers and the associate editor for their constructive comments and criticism.

REFERENCES

[1] H. Burchardt, N. Serafimovski, D. Tsonev, S. Videv, and H. Haas, "VLC: Beyond point-to-point communication," *IEEE Commun. Mag.*, vol. 52, no. 7, pp. 98–105, Jul. 2014.

[2] S. Dimitrov and H. Haas, *Principles of LED Light Communications: Towards Networked Li-Fi*. Cambridge, U.K.: Cambridge Univ. Press, 2015.

[3] A. Jovicic, J. Li, and T. Richardson, "Visible light communication: Opportunities, challenges and the path to market," *IEEE Commun. Mag.*, vol. 51, no. 12, pp. 26–32, Dec. 2013.

[4] H. Haas, L. Yin, Y. Wang, and C. Chen, "What is LiFi?" *J. Lightw. Technol.*, vol. 34, no. 6, pp. 1533–1544, Mar. 15, 2016.

[5] D. Karunatilaka, F. Zafar, V. Kalavally, and R. Parthiban, "LED based indoor visible light communications: State of the art," *IEEE Commun. Surveys Tuts.*, vol. 17, no. 3, pp. 1649–1678, 3rd Quart., 2015.

[6] S. Rajbhandari *et al.*, "High-speed integrated visible light communication system: Device constraints and design considerations," *IEEE J. Sel. Areas Commun.*, vol. 33, no. 9, pp. 1750–1757, Sep. 2015.

[7] E. Sarbazi and M. Uysal, "PHY layer performance evaluation of the IEEE 802.15.7 visible light communication standard," in *Proc. 2nd Int. Workshop Opt. Wireless Commun. (IWOW)*, Oct. 2013, pp. 35–39.

[8] P. H. Pathak, X. Feng, P. Hu, and P. Mohapatra, "Visible light communication, networking, and sensing: A survey, potential and challenges," *IEEE Commun. Surveys Tuts.*, vol. 17, no. 4, pp. 2047–2077, 4th Quart., 2015.

[9] S. K. Nobar, K. A. Mehr, and J. M. Niya, "Comprehensive performance analysis of IEEE 802.15.7 CSMA/CA mechanism for saturated traffic," *IEEE J. Opt. Commun. Netw.*, vol. 7, no. 2, pp. 62–73, Feb. 2015.

[10] Z. Zhang, X. Yu, L. Wu, J. Dang, and V. O. K. Li, "Performance analysis of full-duplex visible light communication networks," in *Proc. IEEE Int. Conf. Commun. (ICC)*, Jun. 2015, pp. 3933–3938.

[11] L. Zhao, X. Chi, and W. Shi, "A QoS-driven random access algorithm for MPR-capable VLC system," *IEEE Commun. Lett.*, vol. 20, no. 6, pp. 1239–1242, Jun. 2016.

[12] J. Dang and Z. Zhang, "Comparison of optical OFDM-IDMA and optical OFDMA for uplink visible light communications," in *Proc. Int. Conf. Wireless Commun. Signal Process. (WCSP)*, Oct. 2012, pp. 1–6.

[13] J. A. Salehi, "Code division multiple-access techniques in optical fiber networks. I. Fundamental principles," *IEEE Trans. Commun.*, vol. 37, no. 8, pp. 824–833, Aug. 1989.

[14] J. A. Salehi and C. A. Brackett, "Code division multiple-access techniques in optical fiber networks. II. Systems performance analysis," *IEEE Trans. Commun.*, vol. 37, no. 8, pp. 834–842, Aug. 1989.

[15] M. F. Guerra-Medina, B. Rojas-Guillama, O. González, J. A. Martín-González, E. Poves, and F. J. López-Hernández, "Experimental optical code-division multiple access system for visible light communications," in *Proc. Wireless Telecommun. Symp. (WTS)*, Apr. 2011, pp. 1–6.

[16] P. V. Kumar, R. Omrani, J. Touch, A. E. Willner, and P. Saghari, "CTH01-5: A novel optical CDMA modulation scheme: Code cycle modulation," in *Proc. IEEE GLOBECOM*, Nov./Dec. 2006, pp. 1–5.

[17] M. F. Guerra-Medina, O. González, B. Rojas-Guillama, J. A. Martín-González, F. Delgado, and J. Rabadán, "Ethernet-OCDMA system for multi-user visible light communications," *Electron. Lett.*, vol. 48, no. 4, pp. 227–228, Feb. 2012.

[18] H. Marshoud, V. M. Kapinas, G. K. Karagiannidis, and S. Muhaidat, "Non-orthogonal multiple access for visible light communications," *IEEE Photon. Technol. Lett.*, vol. 28, no. 1, pp. 51–54, Jan. 1, 2016.

[19] "5G radio access: Requirements, concept and technologies," NTT DOCOMO Inc., Tokyo, Japan, 5G White Paper.

[20] L. Dai, B. Wang, Y. Yuan, S. Han, C.-L. I, and Z. Wang, "Non-orthogonal multiple access for 5G: Solutions, challenges, opportunities, and future research trends," *IEEE Commun. Mag.*, vol. 53, no. 9, pp. 74–81, Sep. 2015.

[21] Z. Ding, Z. Yang, P. Fan, and H. V. Poor, "On the performance of non-orthogonal multiple access in 5G systems with randomly deployed users," *IEEE Signal Process. Lett.*, vol. 21, no. 12, pp. 1501–1505, Dec. 2014.

[22] J. Men and J. Ge, "Non-orthogonal multiple access for multiple-antenna relaying networks," *IEEE Commun. Lett.*, vol. 19, no. 10, pp. 1686–1689, Oct. 2015.

[23] Z. Ding, F. Adachi, and H. V. Poor, "The application of MIMO to non-orthogonal multiple access," *IEEE Trans. Wireless Commun.*, vol. 15, no. 1, pp. 537–552, Jan. 2016.

[24] Z. Ding and H. V. Poor, "Design of massive-MIMO-NOMA with limited feedback," *IEEE Signal Process. Lett.*, vol. 23, no. 5, pp. 629–633, May 2016.
[25] Q. Sun, S. Han, C.-L. I, and Z. Pan, "On the ergodic capacity of MIMO NOMA systems," *IEEE Wireless Commun. Lett.*, vol. 4, no. 4, pp. 405–408, Aug. 2015.
[26] Z. Yang, Z. Ding, P. Fan, and G. K. Karagiannidis, "On the performance of non-orthogonal multiple access systems with partial channel information," *IEEE Trans. Commun.*, vol. 64, no. 2, pp. 654–667, Feb. 2016.
[27] L. Yin, X. Wu, and H. Haas, "On the performance of non-orthogonal multiple access in visible light communication," in *Proc. IEEE 26th Annu. Int. Symp. Pers., Indoor, Mobile Radio Commun. (PIMRC)*, Aug./Sep. 2015, pp. 1354–1359.
[28] L. Yin, W. O. Popoola, X. Wu, and H. Haas, "Performance evaluation of non-orthogonal multiple access in visible light communication," *IEEE Trans. Commun.*, vol. 64, no. 12, pp. 5162–5175, Dec. 2016.
[29] R. C. Kizilirmak, C. R. Rowell, and M. Uysal, "Non-orthogonal multiple access (NOMA) for indoor visible light communications," in *Proc. 4th Int. Workshop Opt. Wireless Commun. (IWOW)*, Sep. 2015, pp. 98–101.
[30] K. Ying, H. Qian, R. J. Baxley, and S. Yao, "Joint optimization of precoder and equalizer in MIMO VLC systems," *IEEE J. Sel. Areas Commun.*, vol. 33, no. 9, pp. 1949–1958, Sep. 2015.
[31] H. Marshoud, D. Dawoud, V. M. Kapinas, G. K. Karagiannidis, S. Muhaidat, and B. Sharif, "MU-MIMO precoding for VLC with imperfect CSI," in *Proc. 4th Int. Workshop Opt. Wireless Commun. (IWOW)*, Sep. 2015, pp. 93–97.
[32] H. Ma, L. Lampe, and S. Hranilovic, "Coordinated broadcasting for multiuser indoor visible light communication systems," *IEEE Trans. Commun.*, vol. 63, no. 9, pp. 3313–3324, Sep. 2015.
[33] J. Gancarz, H. Elgala, and T. D. C. Little, "Impact of lighting requirements on VLC systems," *IEEE Commun. Mag.*, vol. 51, no. 12, pp. 34–41, Dec. 2013.
[34] *IEEE Standard for Local and Metropolitan Area Networks—Part 15.7: Short-Range Wireless Optical Communication Using Visible Light*, IEEE Standard 802.15.7-2011, Sep. 2011, pp. 1–309.
[35] K. Lee and H. Park, "Modulations for visible light communications with dimming control," *IEEE Photon. Technol. Lett.*, vol. 23, no. 16, pp. 1136–1138, Aug. 15, 2011.
[36] I. Stefan, H. Elgala, and H. Haas, "Study of dimming and LED nonlinearity for ACO-OFDM based VLC systems," in *Proc. IEEE Wireless Commun. Netw. Conf. (WCNC)*, Apr. 2012, pp. 990–994.
[37] F. Miramirkhani and M. Uysal, "Channel modeling and characterization for visible light communications," *IEEE Photon. J.*, vol. 7, no. 6, Dec. 2015, Art. no. 7905616.
[38] I. Moreno and C.-C. Sun, "Modeling the radiation pattern of LEDs," *Opt. Exp.*, vol. 16, no. 3, pp. 1808–1819, Feb. 2008. [Online]. Available: http://www.opticsexpress.org/abstract.cfm?URI=oe-16-3-1808
[39] T. Komine and M. Nakagawa, "Fundamental analysis for visible-light communication system using LED lights," *IEEE Trans. Consum. Electron.*, vol. 50, no. 1, pp. 100–107, Feb. 2004.
[40] C. C. Trinca, J.-C. Belfiore, E. D. de Carvalho, and J. V. Filho, "Estimation with mean square error for real-valued channel quantization," in *Proc. IEEE Globecom Workshops (GC Wkshps)*, Dec. 2014, pp. 275–280.
[41] F. Zafar, D. Karunatilaka, and R. Parthiban, "Dimming schemes for visible light communication: The state of research," *IEEE Trans. Wireless Commun.*, vol. 22, no. 2, pp. 29–35, Apr. 2015.
[42] S. H. Lee, S.-Y. Jung, and J. K. Kwon, "Modulation and coding for dimmable visible light communication," *IEEE Commun. Mag.*, vol. 53, no. 2, pp. 136–143, Feb. 2015.
[43] M. Seyfi, S. Muhaidat, and J. Liang, "Amplify-and-forward selection cooperation over Rayleigh fading channels with imperfect CSI," *IEEE Trans. Wireless Commun.*, vol. 11, no. 1, pp. 199–209, Jan. 2012.
[44] M. J. Taghiyar, S. Muhaidat, and J. Liang, "On the performance of pilot symbol assisted modulation for cooperative systems with imperfect channel estimation," in *Proc. IEEE Wireless Commun. Netw. Conf. (WCNC)*, Apr. 2010, pp. 1–5.
[45] J. Liu, N. Kato, J. Ma, and T. Sakano, "Throughput and delay tradeoffs for mobile ad hoc networks with reference point group mobility," *IEEE Trans. Wireless Commun.*, vol. 14, no. 3, pp. 1266–1279, Mar. 2015.
[46] M. Lopez-Benitez and F. Casadevall, "Versatile, accurate, and analytically tractable approximation for the Gaussian Q-function," *IEEE Trans. Commun.*, vol. 59, no. 4, pp. 917–922, Apr. 2011.

Hanaa Marshoud received the bachelor's degree in electrical engineering from Ajman University of Science and Technology, UAE, in 2011, and the M.Sc. and Ph.D. degrees in electrical and computer engineering from Khalifa University, UAE, in 2013 and 2017, respectively. Her research interests include signal processing for wireless and optical wireless communications with a particular focus on visible light communication systems.

Paschalis C. Sofotasios (S'07–M'12–SM'16) was born in Volos, Greece, in 1978. He received the M.Eng. degree from Newcastle University, U.K., in 2004, the M.Sc. degree from the University of Surrey, U.K., in 2006, and the Ph.D. degree from the University of Leeds, U.K., in 2011. He has held academic positions at the University of Leeds, U.K., the University of California at Los Angeles, Los Angeles, CA, USA, the Tampere University of Technology, Finland, Khalifa University, UAE, and the Aristotle University of Thessaloniki, Greece. His M.Sc. studies were funded by a scholarship from UK-EPSRC and his Doctoral studies were sponsored by UK-EPSRC and Pace plc. His research interests are in the broad areas of digital and optical wireless communications as well as in topics relating to special functions and statistics.

Dr. Sofotasios serves as a regular reviewer for several international journals and has been a member of the technical program committee of numerous IEEE conferences. He currently serves as an Editor of the IEEE COMMUNICATIONS LETTERS. He received the Exemplary Reviewer Award from the IEEE COMMUNICATIONS LETTERS in 2012 and the IEEE TRANSACTIONS ON COMMUNICATIONS in 2015 and 2016. He was a co-recipient of the Best Paper Award at ICUFN 2013.

Sami Muhaidat (S'01–M'08–SM'11) received the Ph.D. degree in electrical and computer engineering from the University of Waterloo, Waterloo, ON, Canada, in 2006. From 2007 to 2008, he was an NSERC Post-Doctoral Fellow with the Department of Electrical and Computer Engineering, University of Toronto, ON, Canada. From 2008 to 2012, he was an Assistant Professor with the School of Engineering Science, Simon Fraser University, Burnaby, BC, Canada. He is currently an Associate Professor with Khalifa University, Abu Dhabi, UAE, and a Visiting Professor with the Department of Electrical and Computer Engineering, University of Western Ontario, London, ON, Canada. He is also a Visiting Reader with the Faculty of Engineering, University of Surrey, Guildford, U.K.

Dr. Muhaidat currently serves as a Senior Editor of the IEEE COMMUNICATIONS LETTERS and an Editor of the IEEE TRANSACTIONS ON COMMUNICATIONS. He was a recipient of several scholarships during his undergraduate and graduate studies and the winner of the 2006 NSERC Post-Doctoral Fellowship Competition.

George K. Karagiannidis (M'96–SM'03–F'14) was born in Pithagorion, Samos Island, Greece. He received the University Diploma and Ph.D. degrees in electrical and computer engineering from the University of Patras, in 1987 and 1999, respectively. From 2000 to 2004, he was a Senior Researcher with the Institute for Space Applications and Remote Sensing, National Observatory of Athens, Greece. In 2004, he joined the Faculty of Aristotle University of Thessaloniki, Greece, where he is currently a Professor with the Electrical and Computer Engineering Department and the Director of Digital Telecommunications Systems and Networks Laboratory. He is also an Honorary Professor with South West Jiaotong University, Chengdu, China. He has authored or co-authored over 400 technical papers published in scientific journals and presented at international conferences. His research interests are in the broad area of digital communications systems and signal processing, with emphasis on wireless communications, optical wireless communications, wireless power transfer, and applications, molecular communications, communications and robotics and wireless security. He is also an author of the Greek edition of the book *Telecommunications Systems* and a co-author of the book *Advanced Optical Wireless Communications Systems*, (Cambridge Publications, 2012).

Dr. Karagiannidis has been involved as the general chair, a technical program chair, and a member of technical program committees of several IEEE and non- IEEE conferences. He was an Editor in the IEEE TRANSACTIONS ON COMMUNICATIONS, a Senior Editor of the IEEE COMMUNICATIONS LETTERS, an Editor of the *EURASIP Journal of Wireless Communications and Networks*, and several times a Guest Editor of the IEEE SELECTED AREAS IN COMMUNICATIONS. From 2012 to 2015, he was an Editor-in Chief of the IEEE COMMUNICATIONS LETTERS.

He is a highly cited author across all areas of electrical engineering and was recognized as a Thomson Reuters Highly Cited Researcher in 2015 and 2016.

Bayan S. Sharif (M'92–SM'01) received the B.Sc. degree from the Queen's University of Belfast, U.K., in 1984, the Ph.D. degree from Ulster University, U.K., in 1988, and the D.Sc. degree from Newcastle University, U.K., in 2013. From 1990 to 2012, he was on the Faculty of Newcastle University, U.K., where he held a number of appointments, including Professor of Digital Communications, the Head of Communications and Signal Processing Research, and the Head of the School of Electrical, Electronic and Computer Engineering. He is currently the Dean of the College of Engineering, Khalifa University, Abu Dhabi, UAE. His main research interests are in digital communications with a focus on wireless receiver structures and optimization of wireless networks. He is a chartered engineer and a fellow of the IET, U.K.